Dynamic Polar Solvation Is Reported by Fluorescing 4-Aminophthalimide Faithfully Despite H-Bonding

Mohsen Sajadi,[†] Thorsten Obernhuber,[‡] Sergey A. Kovalenko,[†] Manuel Mosquera,[§] Bernhard Dick,*[,‡] and Nikolaus P. Ernsting*[,†]

Department of Chemistry, Humboldt University, Berlin, Germany; Department of Physical and Theoretical Chemistry, Faculty for Chemistry and Pharmacy, University Regensburg, Germany; and Department of Physical Chemistry, University of Santiago de Compostela, Spain

Received: August 26, 2008; Revised Manuscript Received: October 20, 2008

Solvation dynamics of 4-aminophthalimide (4AP) in methanol is measured by broadband upconversion of the fluorescence band. The peak emission frequency $\tilde{\nu}(t)$ is determined from 100 fs onward with 85 fs time resolution. Polar solvation based on simple continuum theory, including solute polarizability, describes the temporal shape of $\tilde{\nu}(t)$ quantitatively. Extrapolation $\tilde{\nu}(t\rightarrow 0)$ points to an initial emission frequency which agrees with the result from stationary spectroscopy in a nonpolar solvent. The extent (4300 cm^{-1}) of the dynamic Stokes shift is largely due (50%) to H-bonding, however. The observations imply that H-bonds with 4AP adiabatically follow the dielectric relaxation of the methanol network. The stimulated emission band is also used to measure solvation dynamics. The evolving band is monitored by transient absorption spectroscopy of supercontinuum probe pulses. But the excited-state absorption spectrum, its relative amplitude, and its evolution are needed to extract $\tilde{\nu}(t)$ from such measurements. These key data are obtained by comparison with the upconversion results. Thus calibrated photometrically, 4AP transient absorption can be used to monitor solvation dynamics in any solvent. The excited-state absorption spectrum is assigned with the help of time-dependent density-functional calculations. Fluorescence excitation and double-resonance spectroscopy of isolated 4AP, cooled in a supersonic jet, is used to determine optically active modes. An intramolecular reorganization energy is inferred which is consistent with the value in 2-methylbutane (2025 cm^{-1}). The crystal structure is also provided.

1. Introduction

4-Aminophthalimide (4AP, inset to Figure 1) and derivatives are widely used as fluorescent probes in complex media like cyclodextrins,[1] micelles,[2] ionic solutions,[3] ionic liquids,[4] and polymers[5] (citing examples where further references can be found). A long radiative lifetime,[6] large Stokes shift depending on solvent,[6,7] acceptable fluorescence quantum yield,[6] and absence of interfering excited states[8] render these probes useful for studying the polarity of the environment. In protic solvents, the fluorescence lifetime decreases and the Stokes shift increases remarkably[9] compared to nonprotic solvents of the same polarity. The last point is illustrated in Figure 1 where the peak position of the absorption and fluorescence line shapes (see below) of 4AP are plotted against solvent polarity. The peaks in alcohols and water (black dots) stray below the regression lines for nonhydroxylic solvents[6] (colored dots) by ~1000 and 3000 cm^{-1} for absorption and emission, respectively. Since methanol is examined in this work, its deviations are marked especially by vertical lines. This general behavior has been discussed intensely, and for a summary the reader is referred to ref 9. The large Stokes shift in protic solvents was attributed to differences in H-bonding between the S_1 and S_0 states, rather than to the difference between dipole moments.[7,9] Solvent-mediated proton transfer is another explanation,[10] supported by a comparison of photophysical properties in H_2O and D_2O.[11] A flash photolysis study showed that enhanced internal conversion is responsible for the decrease of fluorescence lifetime in protic solvents.[12]

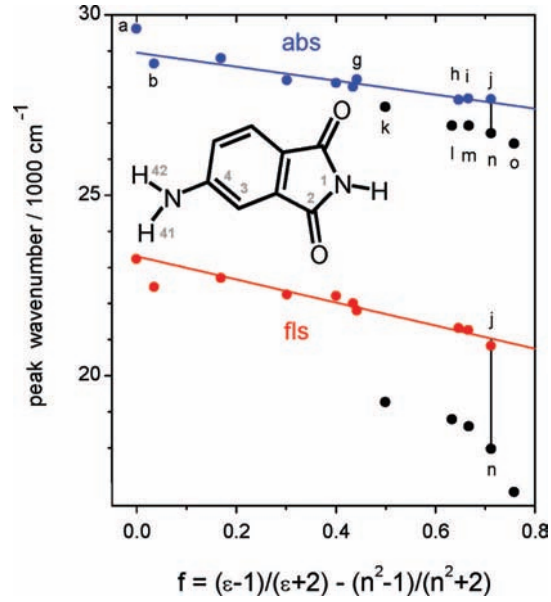

Figure 1. Solvatochromism of 4AP: peak position of absorption and fluorescence line shapes (corrected for dispersive shifts) against polarity *f*.[6] Colored, a−j: cyclohexane, dioxane, dibutyl ether, diethyl ether, ethyl acetate, methyl acetate, THF, DMF, acetone, acetonitrile. Black, k−o: *n*-octanol, *n*-propanol, ethanol, methanol, water. Vertical lines mark the deviation of 4AP in methanol from nonspecific polar behavior, represented by acetonitrile solutions.

* To whom correspondence should be addressed. E-mail: bernhard.dick@chemie.uni-regensburg.de, nernst@chemie.hu-berlin.de.
[†] Humboldt University.
[‡] University Regensburg.
[§] University of Santiago de Compostela.

10.1021/jp807605b CCC: $40.75 © 2009 American Chemical Society
Published on Web 12/15/2008

The solvation dynamics of 4AP (and other dyes) in 1-propanol has been measured with 20 ps time resolution.[13] The spectral relaxation of the fluorescence band at 253 K was found to obey theories for nonspecific solvation despite the energetic importance of hydrogen bonding. For *N*-methyl-4AP in *n*-butanol and *n*-decanol the relaxation dynamics at 298 K is roughly given by the longitudinal relaxation time of simple continuum theory.[14] Similar work on 3-AP in *n*-butanol reached the same conclusion.[15] In complex media the solvation dynamics of 4AP is slower compared to pure solvents.[16−18]

Here we examine 4AP in methanol at room temperature. Broadband fluorescence upconversion[19−22] enables higher temporal and photometric resolution than before,[23,24] and thus the question of molecularity is posed anew: can the reorganization of H-bonds be observed directly? We find that polar solvation based on simple continuum theory describes the temporal shape of $\tilde{\nu}(t)$ quantitatively. Extrapolation of $\tilde{\nu}(t\rightarrow 0)$ points to an initial emission frequency which agrees with the time-zero result from stationary spectroscopy. Therefore, an H-bond is not required *as dynamic variable* in the solvation process following optical excitation.

Transient absorption with supercontinuum probing[25,26] provides an alternative means for observing the dynamic Stokes shift of fluorescence. The band for stimulated emission is monitored in this case. The method is technically easier than broadband upconversion; it was used recently to characterize the early solvation dynamics in oligonucleotides.[27,28] But the measurements are less accurate to evaluate because the desired band for stimulated emission is overlaid by the induced spectra of ground-state bleaching and excited-state absorption, and their separation is not unique. Here, transient absorption spectra for 4AP in methanol are photometrically "calibrated" by comparison with the upconversion results. An excited-state absorption spectrum, its relative amplitude, and time evolution are obtained, and a prescription for the photometric correction in any solvent is given. The excited-state absorption spectrum is assigned with the help of time-dependent density-functional calculations.

The vibronic structure of the molecular probe, isolated at low temperature in a supersonic jet, is also relevant for solvation dynamics. Thus C153 was shown to have several conformations of the amino group.[29,30] The population flow between these conformations alters the shape of the emission band and thereby influences the dynamic Stokes shift. In an ideal probe the electronic chromophore should be rigid, i.e. the intramolecular reorganization energy after $S_1 \leftarrow S_0$ excitation should be small, confined to a few modes of a single isomer, and the modes should be identical in the S_1 and S_0 states. These conditions can be tested most directly by laser-induced fluorescence spectroscopy in a supersonic jet. Early work on *N*-methyl-4APs showed that the vibrational levels in S_1 are organized in a few optically active modes only.[31,32] Microsolvation of isolated 4AP by one or two methanol molecules confirmed the strong coupling via H-bonds.[29] Here we examine isolated 4AP cooled in a supersonic jet. Optical–optical double resonance spectroscopy is used to determine 16 optically active modes. An intramolecular reorganization energy is inferred which is consistent with the value in 2-methylbutane.

2. Experimental Section

Materials. 4AP (Acros) was sublimed; melting point 290.7 °C. Crystals for X-ray diffraction (see Supporting Information) were obtained from a solution in methanol upon slow evaporation. Solvents were of spectroscopic quality (Merck Uvasol). For fluorescence spectroscopy in 2-methylbutane, the solvent was degassed and dried over granulated sodium in a sealed vessel, previously dried under high vacuum, with a sample cell attached for optical measurements. All measurements were carried out at 21 ± 0.5 °C.

Absorption and emission spectra were recorded on a Cary 300 spectrometer and a Spex 212 fluorometer, respectively, with bandwidth ≤2 nm. Wavelengths were calibrated to ±0.1 nm with a holmium glass filter or a Hg lamp. Fluorescence was compared to the emission of a secondary standard lamp (Gigahertz Optic Model BN9701), and background from the pure solvent was always subtracted. The absorption spectrum in 2-methylbutane is approximated by the excitation spectrum recorded with 420 nm detection. Excitation at 350 nm was used for the fluorescence spectrum in 2-methylbutane.

Broadband fluorescence upconversion was performed with the setup of ref 22. Fluorescence of 4AP in methanol was excited by focusing 4 μJ, 403 nm pump pulses (repetition rate 500 Hz) to a spot diameter 50−80 μm in a sample flow cell having 150 μm internal path length. In order to avoid reabsorption of fluorescence from the excited state,[21] an optical density OD = 0.3 at the pump wavelength was chosen, corresponding to a concentration of 11.8×10^{-3} mol/L. The collected emission was approximately imaged 1:7 onto a KDP crystal (0.2 mm, cut at 65°) for type II sum-frequency generation with 60 μJ, 1.3 μm gate pulses. By increasing the angle between the central fluorescence ray and the gate beam from 14°[22] to 20°, the upconverted fluorescence spectrum was obtained completely background-free, without long-pass filter in the fluorescence beam. The dispersion on the CCD camera (Andor Newton) was 10 cm^{-1}/pixel on average. A time resolution of 85 fs (fwhm of pump-gate intensity cross correlation measured with upconverted Raman light) was achieved by tilting the gate pulses.[22] Transient fluorescence spectra were recorded (10 s integration time) in 10 fs steps until pump-gate delays of 3 ps, and in 200 fs steps until 40 ps. For each kind, the results from 8 time scans were averaged. Photometric calibration was performed with the dyes 4AP, Coumarin 6H, and 2,5-bis[5-*tert*-butylbenzoxazolyl(2)]thiophene in methanol at a delay of 150 ps after the pump pulse. The time correction for group-velocity dispersion of the fluorescence was calculated from material dispersions (cell window of 200 μm fused silica, and Moxtec polarizer on 700 μm 1737F Corning glass). All measurements were carried out with pump and detection polarizations at magic angle.

Transient absorption was measured by pump−supercontinuum probe spectroscopy in the setup of ref 33 with 0.6 μJ, 403 nm pump pulses. Single-shot absorption spectra were acquired at 250 Hz, and 50 such spectra were averaged for a recorded spectrum. The time resolution of this experiment was 65 fs (fwhm). Time steps were 6 and 100 fs, each with parallel, perpendicular, and magic-angle setting of the pump and probe polarizations. The corresponding time correction was obtained from measurements with pure methanol.[34] Finally, the results from 20 time scans were averaged.

Fluorescence Excitation in a Supersonic Jet. The apparatus for the generation of supersonic beams was described earlier.[35] Experiments were performed with He carrier gas at a stagnation pressure of 2.0−2.5 bar. Fluorescence excitation and optical−optical double resonance (OODR) spectra were recorded with the laser setup described in ref 36. For OODR measurements, two dye-laser beams were arranged counterpropagating, separated by 1.5 mm, crossing the supersonic jet ca. 6 mm downstream from the pulsed nozzle (General Valve No. 9 operated at 204 °C). Two photomultipliers were used, one on each side of the axis perpendicular to the plane spanned by the

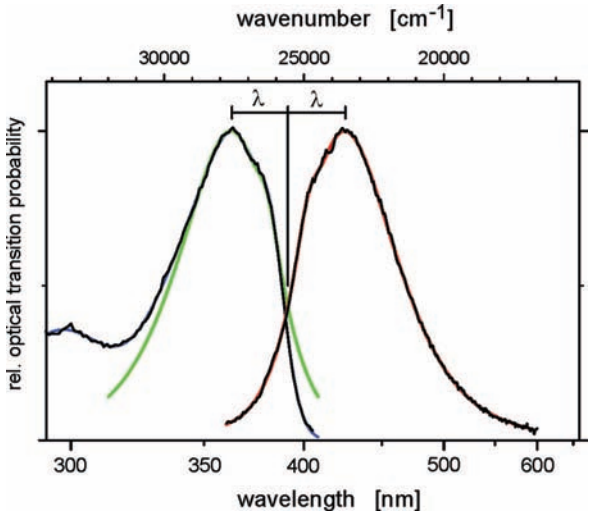

Figure 2. Optical line shapes of 4AP in 2-methylbutane, calculated from the fluorescence excitation and fluorescence spectra (see text). Blue and red lines indicate fits by log-normal functions; the green line was obtained by reflecting the emission band at 25 580 cm^{-1}. The classical intramolecular reorganization energy is represented by $\tilde{\lambda} =$ 2025 cm^{-1}.

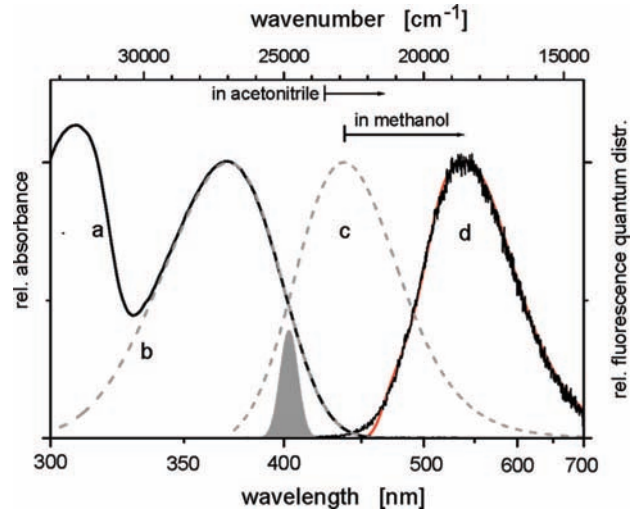

Figure 3. Low-energy absorption spectrum (a) and fluorescence quantum distribution over energy (d) of 4AP in methanol. The $S_1 \leftarrow S_0$ band (b) and the fqd at time-zero (c) were obtained by comparison with the spectra in 2-methylbutane.[8] Arrows indicate the dynamic Stokes shift following 40 fs excitation in methanol (4300 cm^{-1} for $\lambda_{exc} = 403$ nm as indicated) or acetonitrile (2160 cm^{-1}, for equivalent $\lambda_{exc} = 388$ nm).

molecular beam and the laser beams. One collected the fluorescence produced by both laser beams, whereas the other detected only the fluorescence produced by the probe beam. Filters (Schott GG 385) were used to suppress scattered laser light. Fluorescence signals were normalized to the pulse energy of the exciting laser.

Computational Methods. The geometry of the electronic ground state of 4AP was optimized with the density functional theory (DFT) method. The B3LYP functional and the Gamess program[37] in the implementation for Windows[38] were used throughout. Two basis sets, cc-pVDZ and aug-cc-pVDZ, were used to check for convergence. The geometry of the S_1 state was optimized with the CI-singles method. Gas-phase dipole moments were obtained, at the optimized geometries of S_0 and S_1, by state-averaged CASSCF(2,2) calculations followed by MC-QDPT2 (multiconfiguration quasi-degenerate second-order perturbation theory).[39]

3. Results

3.1. Stationary Solution Spectra and Computational Results. Intramolecular reorganization after $S_1 \leftarrow S_0$ excitation is studied in a nonpolar solvent. Figure 2 shows the absorption and fluorescence bands of 4AP in 2-methylbutane. In order to expose mirror symmetry we present the distributions of the optical transition probability, or line shapes, $\propto \varepsilon(\tilde{\nu})/\tilde{\nu}$ and $\propto$ fqd$(\tilde{\nu})/\tilde{\nu}^3$. Here $\varepsilon(\tilde{\nu})$ is the molar extinction coefficient and fqd$(\tilde{\nu})$ the fluorescence quantum distribution over energy.[40] Each line shape is described by a sum of log-normal functions[41] (see Supporting Information). From that description one finds that vibrational structure is due to a mode of 1370−1400 cm^{-1}. By superimposing a reflected emission band onto the absorption band, the electronic origin $S_1(\upsilon'=0) \leftarrow S_0(\upsilon''=0)$ in 2-methylbutane is located at 25 575 ± 30 cm^{-1}. Referring to the peak positions, the intramolecular reorganization energy is $\tilde{\lambda}_{intra} \approx$ 2025 cm^{-1}.

The stationary absorption (a) and fluorescence (d) spectra of 4AP in methanol are shown in Figure 3. Here and from now on, spectra are shown proportional to the extinction coefficient or the fluorescence quantum distribution over energy. The lowest absorption band peaks at 27 040 cm^{-1} and the fluorescence at 18 550 cm^{-1} (from log-normal[41] fits which are collected in the Supporting Information); the Stokes shift between them exceeds 8400 cm^{-1}. From a dynamic perspective, the reorganization process following ultrafast excitation can be envisaged in two stages: (i) intramolecular vibrational redistribution such that the excited molecule attains thermal equilibrium internally, followed by (ii) solvent relaxation[8] and cooling. Note that the solvent must effectively be frozen during step (i). The "time zero" emission band after (i) and before (ii) can be estimated by comparing with the spectra in 2-methylbutane.[8] By this method, we obtain[42] the gray dashed line (c) which peaks at 22 850 cm^{-1}. The "dynamic Stokes shift" consists of the spectral relaxation from here to the stationary fluorescence band; it is indicated in the figure by a horizontal arrow of 4300 cm^{-1} for methanol. Hydrogen bonds are much less developed in acetonitrile,[43] which is why the dynamic Stokes shift amounts only to 2160 cm^{-1} in this solvent (small arrow).[44] Finally, for this part, we return to the absorption spectrum in methanol. The two lowest bands are overlaid in the UV region, but it is possible to identify the $S_1 \leftarrow S_0$ absorption band (b) by comparison with the fluorescence excitation spectrum in 2-methylbutane.

The experimental structure from X-ray diffraction and the optimized structures for S_0 (DFT) and S_1 (CIS) are compared in the Supporting Information. S_0 exhibits a small pyramidal angle (13°) at the amino group.[45] Comparison of the calculated and experimental structural parameters shows that bond lengths between non-hydrogen atoms deviate by 0.015 Å rms between the two sets. Bond angles involving O1, O2, and H1 deviate by ∼0.8°−1.5°, which can be explained as the effect of crystal packing (see Supporting Information). S_1 is predicted to be exactly planar.

When the molecule is constrained to planarity, the optimized S_0 structure is found (by DFT) only 150 cm^{-1} higher in energy compared to the fully relaxed structure. The former is therefore used as reference point for TD-DFT calculations of electronic transition energies, allowing to classify the transitions as A′ and A″ in the C_s point group. Calculated transitions from the electronic ground state are compared in Figure 4 to the absorption spectrum in methanol. Absorptive transitions, indi-

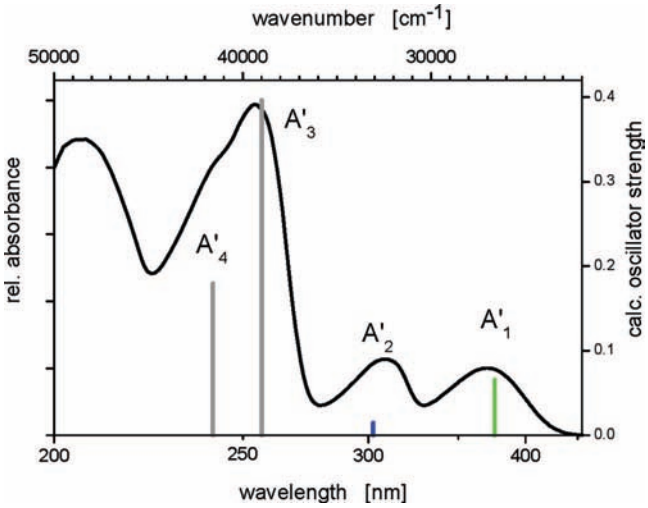

Figure 4. Absorption spectrum in methanol, and oscillator strengths for transitions to excited states A'_i (vertical bars, see Table 1) from time-dependent density-functional theory. The calculated transition frequencies were reduced by 2000 cm^{-1} for the comparison.

TABLE 1: Electronic States of 4AP Constrained to Planarity, in Vacuo, from TD-DFT Calculations (See Text): Transition Frequency $\tilde{\nu}$ and Oscillator Strength f for Optical Transition from the Ground State[a]

		$\tilde{\nu}$ (cm^{-1})	f (−)
A'_0		0	—
A'_1		28630	0.0656
	A''_1	31060	0.0000
A'_2		35080	0.0293
	A''_2	36250	0.0000
	A''_3	38770	0.0022
A'_3		41000	0.3963
	A''_4	42020	0.0000
A'_4		43580	0.1795
	A''_5	44650	0.0015
	A''_6	45720	0.0020

[a] A′ and A″ refer to even or odd symmetry of the electronic wave function upon reflection in the molecular plane.

SCHEME 1: Calculated Coordinates and Dipole Moments of 4AP[a]

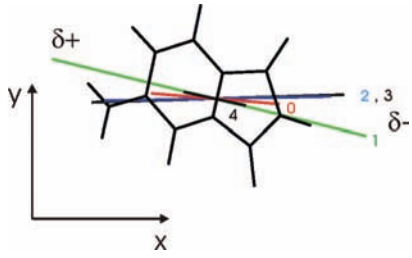

[a] Labels $i = 0-4$ correspond to A'_i states in Figure 4 and Table 1.

cated by a vertical bar representing oscillator strength, are specified in Table 1. The calculations predict 28 630 cm^{-1} for $S_1 \leftarrow S_0$ excitation, while the electronic origin in the isolated molecule is found experimentally at 28 968 cm^{-1} (see below). We conclude that energies in this way are accurate to within numerical precision (dipole moments are overestimated[46]). State-averaged CASSCF(2,2) calculations followed by an MC-QDPT2 predict dipole moments of 5.0 D for S_0 and 10.6 D for S_1. The direction of dipole moments in the molecular frame is shown in Scheme 1. In solution, transition energies are modified by dispersive and polar interactions. To account for this effect, all calculated transition energies were reduced by 2000 cm^{-1}, in which case excellent agreement with the absorption spectrum in methanol is obtained.

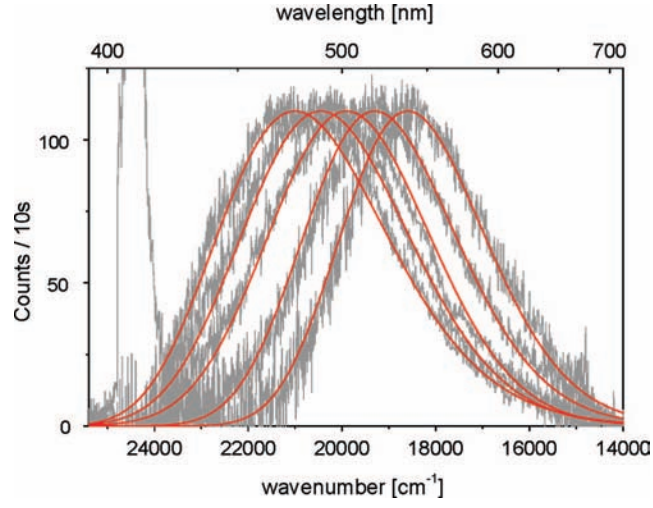

Figure 5. Transient fluorescence spectra in methanol, from broadband upconversion. Quantum distributions at $t = 0.3$, 1, 2.75, 10, and 40 ps (gray lines) are averages of 8 measurements, each with 10 s integration time. Log-normal[40] fits are indicated by red lines.

3.2. Time-Resolved Stokes Shift in Methanol. The power spectrum of the 40 fs excitation pulse is also shown in Figure 3. It intersects the absorption and time-zero emission bands and is thus centered on the electronic origin transition in methanol. Optical excitation should lead to minimal excess vibrational energy in S_1. The time evolution of the excited population is reflected in the basic experimental Figures 5 and 8.

Broadband Fluorescence Upconversion. Transient fluorescence spectra at 0.3, 1, 2.75, 10, and 40 ps are shown in Figure 5. Observing entire spectra directly allows to assess the limits of the method, i.e., the factors which determine the accuracy of finding the peak or average emission frequency. The upconverted fluorescence at 0.3 ps is free of Raman signal due to a short (85 fs) apparatus function. A line at 407 nm belongs to a very weak satellite to the pump pulse. It hampers the analysis in the pump spectral region at early delay times but has practically no consequence for the population inversion. Remember that no filters were used, and the efficiency extends well across the 11 000 cm^{-1} range shown.

Transient fluorescence quantum distributions were fitted by a log-normal function[41] having peak frequency $\tilde{\nu}_p$, width parameter Δ, asymmetry parameter γ, and amplitude h. The resulting smooth spectra are shown as red lines in Figures 5. Their peak frequencies $\tilde{\nu}_p(t)$ are entered as red points into Figure 6, and the frequency relaxation is described by a multiexponential fit to the data (green lines). A rms deviation of 40 cm^{-1} can be regarded as the precision of the measurement.[47] Horizontal lines mark the stationary state where $\tilde{\nu}_p(\infty) = 18\,550$ cm^{-1}. The first spectrum which can be analyzed with confidence has $\tilde{\nu}_p(100\text{ fs}) = 21\,540$ cm^{-1}. Figure 7 shows the temporal behavior of the width and asymmetry parameters. For comparison, the frequency relaxation curve (red line) was copied from the previous figure. The amplitudes and decay times from all multiexponential fits are gathered in Table 2. Deconvolution of the transient fluorescence spectra with the apparatus function has no effect for $t \geq 150$ fs (see below).

Transient absorption with supercontinuum probing is shown in Figure 8. A wide spectral range, from 300 to 700 nm, is plotted against wavelength since this is how the spectra are registered in the experiment. Fluorescence now appears as

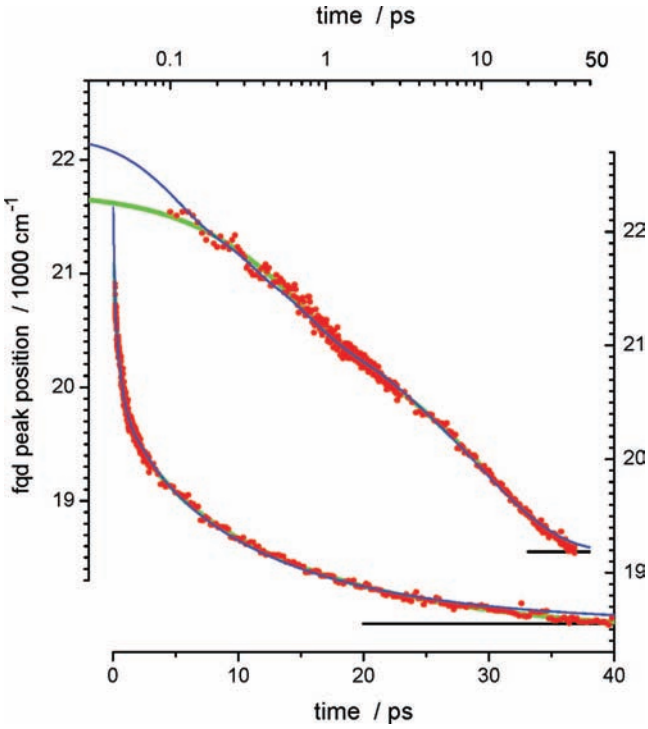

Figure 6. Relaxation of the fluorescence (fqd) peak. Dots mark the peak of the red spectra in Figure 5, and horizontal lines indicate the final frequency $\tilde{\nu}(\infty)$. Green lines, multiexponential fit; blue lines, dielectric relaxation according to continuum theory ($\alpha_1 = 18.2$ Å^3; see Discussion and compare Figure 14).

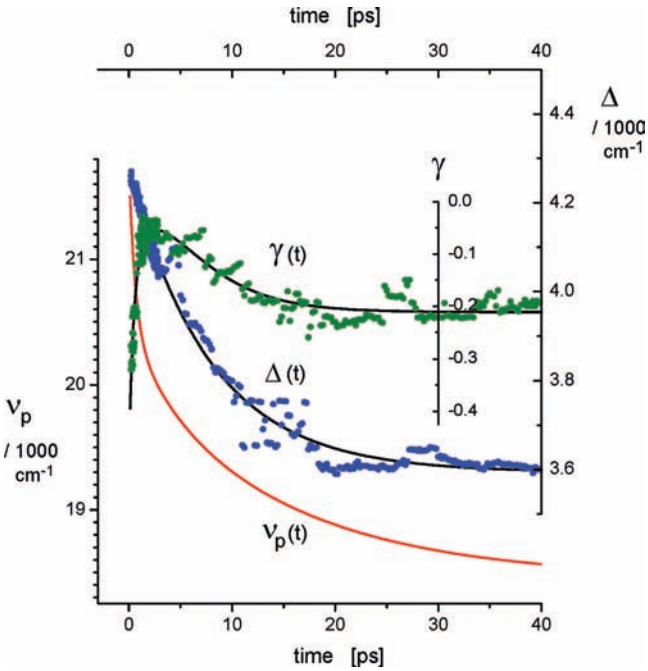

Figure 7. Fluorescence width (Δ) and asymmetry (γ) parameters. Points represent measurement and black lines a multiexponential fit (Table 2). The $\tilde{\nu}_p$ relaxation curve from Figure 6 is shown for comparison (red line).

stimulated emission (SE) in a band with negative induced optical density, ΔOD < 0, around 500 nm. Bleach (BL) is recognized briefly as ΔOD < 0 around 400 nm. Excited-state absorption (ESA) dominates the UV region and contributes a broad background in the red. The evolution of the characteristic features is indicated by arrows; it consists mainly of a red shift of the SE band and rise of ESA in the UV. The results will be

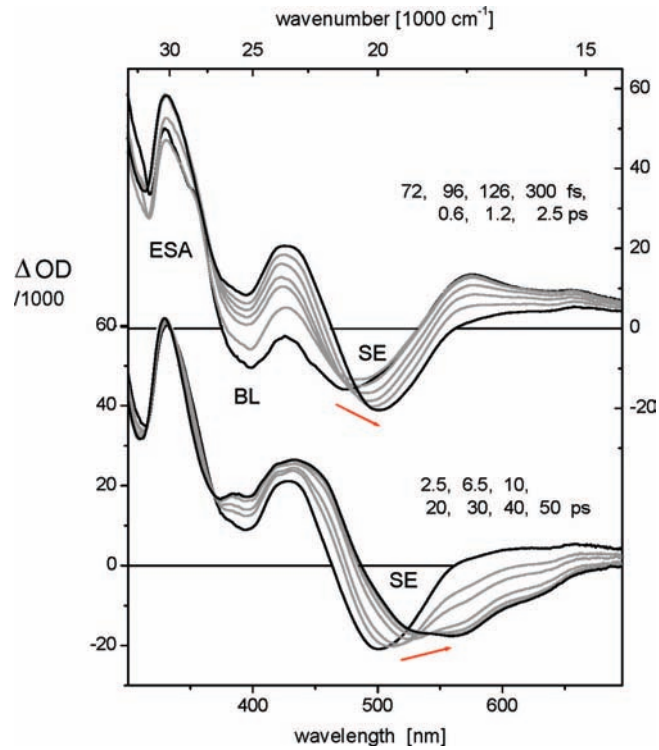

Figure 8. Transient absorption spectra in methanol, following optical excitation at 403 nm. Negative induced optical density ΔOD < 0 indicates bleach (BL) and stimulated emission (SE) in the absorption and fluorescence regions, respectively, while ΔOD > 0 corresponds to excited-state absorption (ESA). The rms noise of the raw data shown here is $<3 \times 10^{-4}$.

examined from two angles. First, we see how accurately the dynamic Stokes shift in methanol can be extracted, using the fluorescence results for guidance. We also suggest a practical extraction procedure for use with any solvent. In a second approach, the excited-state absorption and its spectral evolution are determined for comparison with quantum-chemical calculations.

In order to extract the dynamic Stokes shift, the stimulated emission band in every transient spectrum must be estimated. The procedure, which has been described already,[25,26] is outlined here for consistency. We begin with the stationary absorption spectrum σ_{Abs} which is considered to be normalized at the peak of the $S_1 \leftarrow S_0$ band. A transition-dipole-squared, $M^2 = \int \sigma_{10}/\tilde{\nu}\, d\tilde{\nu}$, is determined where σ_{10} represents the $S_1 \leftarrow S_0$ band (Figure 3, dashed line b).[40] Then, from the stationary fluorescence, the band for stimulated emission at late time (symbolized by $t = \infty$) is derived, $\sigma_{SE}(\infty) \propto \text{fqd}(\tilde{\nu})/\tilde{\nu}^2$, and normalized to the same M^2 also. We now possess a trial spectrum $\sigma_{AbsSE}(\infty) = \sigma_{Abs} + \sigma_{SE}(\infty)$. When $\alpha\sigma_{AbsSE}(\infty)$ is subtracted from a transient absorption spectrum measured at late time, the contribution $\Delta OD_{ESA}(\infty)$ should remain. The contribution due to bleaching is of course $\Delta OD_{BL} = \alpha\sigma_{Abs}$. The bleach amplitude α was not measured directly in our experiments. This parameter must be estimated, for example by the condition that $\Delta OD_{ESA}(\infty) \geq 0$ everywhere. For the moment, let us assume that ΔOD_{BL} and $\Delta OD_{ESA}(\infty)$ are known. The next assumption concerns the evolution of excited-state absorption. For laser dyes such as 4AP the ESA contribution is relatively weak in the emission region and without prominent structure (see below). Under such conditions, subtraction of $\Delta OD_{BL} + \Delta OD_{ESA}(\infty)$ from a measured transient absorption spectrum should give the instantaneous stimulated emission band $\Delta OD_{SE}(t,\tilde{\nu}) \leq 0$. The spectral position $\tilde{\nu}(t)$ is determined from a quadratic fit of the band around its minimum.

TABLE 2: Time Dependence of the 4AP Emission Band in Methanol, from Broadband Transient Absorption and Fluorescence Upconversion[a]

		a_1/cm^{-1}	a_2/cm^{-1}	a_3/cm^{-1}	a_4/cm^{-1}	a_5/cm^{-1}	τ_1/ps	τ_2/ps	τ_3/ps	τ_4/ps	τ_5/ps	a_0/cm^{-1}	$\langle\tau\rangle$/ps
transient absorption	SE $\tilde{\nu}_p$	1922	1730	−3242	−	−	0.300	9.27	−532	−	−	21786	6.12
fluorescence upconversion	fqd $\tilde{\nu}_p$	1235	454	1579	−102	−	0.594	3.84	15.4	5000	−	18550	6.56
	Δ	882.4	−449	−	−	−	10.25	58.46	−	−	−	3830	−
	γ	−20.7	38.6	−18.9	5.07	−4.36	1.29	1.47	1.70	9.04	10.1	−0.179	−

[a] Spectral parameters y were fitted by $y = a_0 + \sum_{i=1}^{n} a_i \exp(-t/\tau_i)$, applicable to $0 \le t \le 40$ ps. Entries have no meaning by themselves. For $y \equiv \gamma$ and Δ, large amplitudes of opposite sign with close-lying time constants are needed to capture rise-and-fall behavior. The average solvation time is $\langle\tau\rangle = (y(0) - y(50\text{ ps}))^{-1} \int_0^{50} (y(t) - y(50\text{ ps}))\, dt$ for $y \equiv \tilde{\nu}_p$.

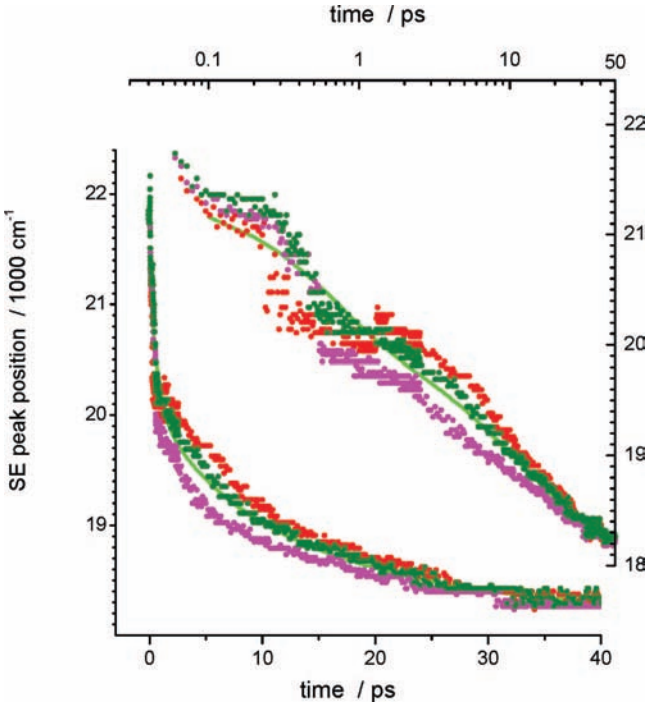

Figure 9. Relaxation of the SE peak in Figure 8, for different estimates of the bleach amplitude α (red, 29 mOD; olive, 34 mOD; magenta, 43 mOD). The green line represents the evolution which is calculated from the fluorescence upconversion results (corresponding to the green line in Figure 6).

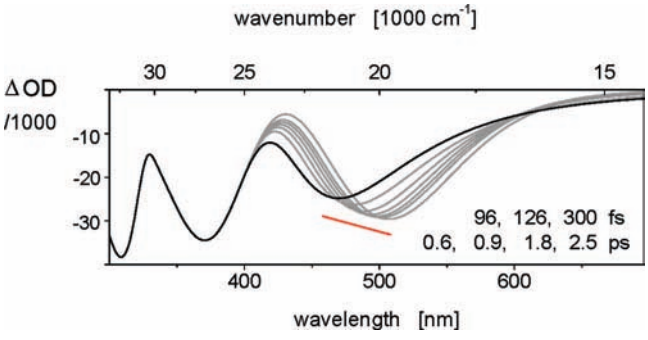

Figure 10. Contributions to transient absorption (Figure 8) due to bleach (BL) and stimulated emission (SE). The simulation uses stationary absorption and time-resolved fluorescence data, and $\beta = 34$ mOD.

Results are shown as dots in Figure 9 for different estimates of the bleach amplitude α. The green line represents the evolution which is calculated (because band shapes differ) from the fluorescence upconversion results; it is taken to represent the evolution of the emission band accurately for the purpose. The deviation between dots and line is lowest with $\alpha = 34 \times 10^{-3}$, amounting to 110 cm^{-1} rms. However, note that the minimal average error is unevenly distributed, with systematic deviations by +300 cm^{-1} (7% of the total dynamic shift) around 200 fs, and by −300 cm^{-1} around 0.6 ps. In principle, the residuals could indicate that an oscillatory solvation process is observed by transient absorption, due to its superior time resolution, which was not resolved by fluorescence upconversion. But the excursions seen in Figure 9 are not expected from model calculations (below) when the time resolution is increased; besides, they would be time resolved by our fluorescence measurements. It follows that the residuals represent a systematic error of the method. A distinction of specific and nonspecific solvation processes can not be made by transient absorption measurements, even though the average solvation time is well determined (Table 2).

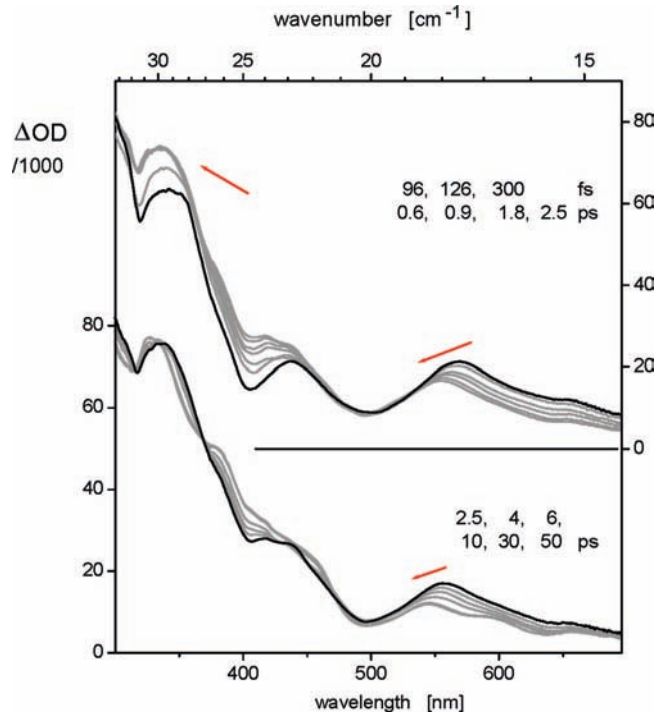

Figure 11. Contribution to transient absorption from excited-state absorption, obtained by subtracting from measurement (Figure 8) the corresponding bleach/stimulated emission spectrum (Figure 10).

For any solvent, the previous comparison of 4AP transient absorption and fluorescence spectroscopies in methanol may serve to "calibrate" the amplitude of the trial spectrum $\sigma_{AbsSE}(\infty)$ which was defined earlier. Note that the optimal value of α is related to the ΔOD signal in the quasi-stationary state ($t = \infty$): 55% of the peak at 330 nm, or 194% of the broad minimum at 560 nm. A similar analysis with 4AP in acetonitrile (not shown) suggests that this relationship can be extended to nonprotic solvents. Tracing backward one obtains the partial spectra $\Delta OD_{BL} + \Delta OD_{ESA}(\infty)$ and further, approximately, the time-dependent band for stimulated emission.

Excited-state absorption in methanol may be obtained by combining transient absorption and fluorescence spectra more

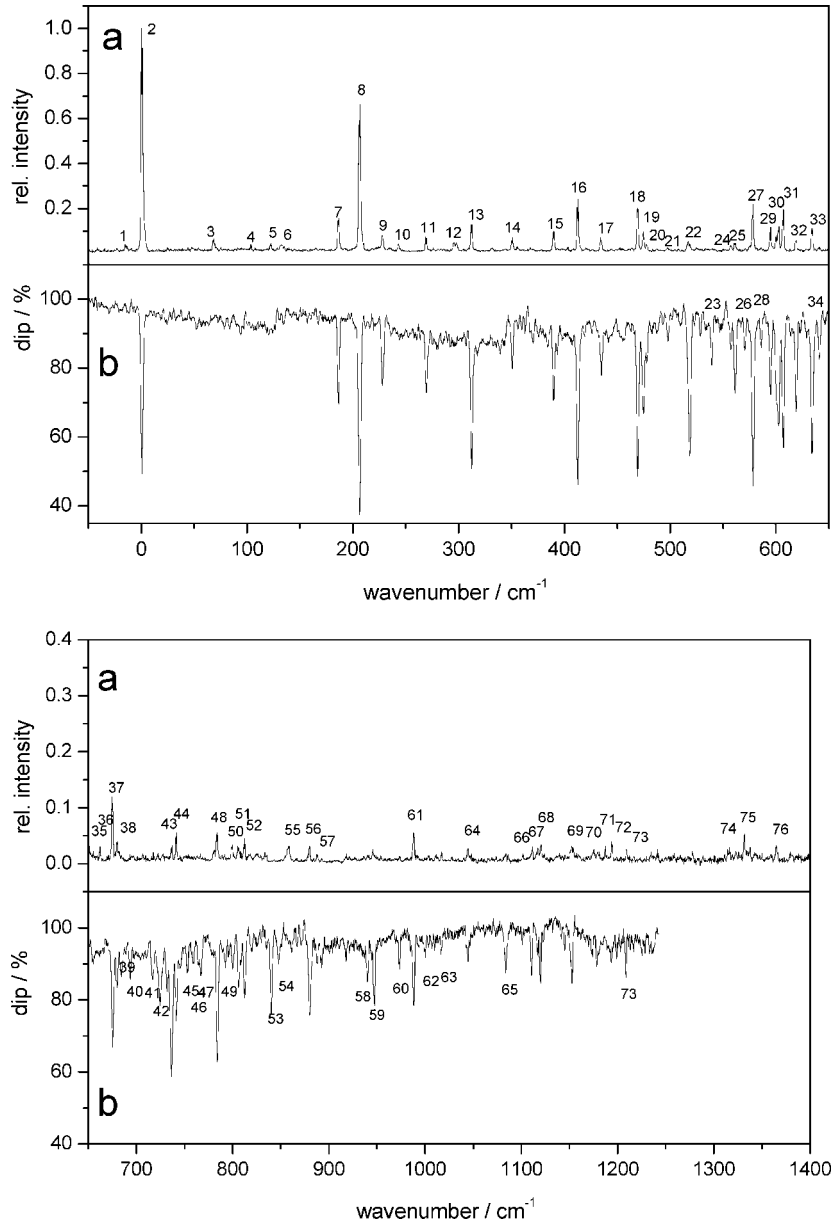

Figure 12. Fluorescence excitation spectrum of isolated 4AP cooled in a supersonic expansion of helium (upper panel), and fluorescence dip in an optical−optical double resonance experiment (lower panel, see text; line labels refer to Table 3).

directly. Before, only the stationary spontaneous emission spectrum was needed, but now we make use of every fqd(t). From the latter one calculates $\sigma_{SE}(t)$ and reaches $\sigma_{AbsSE}(t) = \sigma_{Abs} + \sigma_{SE}(t)$, describing the shape of the joint contribution from bleach and stimulated emission at time t (remember that $\sigma_{AbsSE}(\infty)$ was introduced already). These time-dependent spectra are shown in Figure 10, after scaling by some β. Subtraction from the measured data yields the transient ESA spectra which are shown in Figure 11. An optimal bleach amplitude β may be found by monitoring spectro-temporal properties. For example consider the blue shift of the ESA band at 560 nm which seems to mirror the red shift of the emission band, probably because the corresponding $S_n \leftarrow S_1$ transition decreases the dipole moment.[25,26] By making the temporal shapes of the two opposing shifts agree, we find the same value which was used above. The excited-state absorption spectra in Figure 11 will be assigned in the discussion.

3.3. Vibrational Activity in the Isolated Molecule. The fluorescence excitation spectrum of 4AP seeded into a supersonic beam is shown in the upper parts of Figure 12a,b. The electronic origin $S_1(v'=0) \leftarrow S_0(v''=0)$ is observed at 28 968.0 cm^{-1}, and the excitation range extends 1400 cm^{-1} above. This spectrum was measured at high laser intensity so that some lines were partially saturated. With low laser intensity, only the lines labeled 2, 8, 16, 18, and 27 were observed above the noise level up to an excess energy of 600 cm^{-1}.

Optical−optical double-resonance (OODR) spectroscopy was used to identify all lines that originate from the vibrationless ground state $v'' = 0$. In this experiment, a weak probe laser drives the origin transition and the resulting fluorescence is collected. But ~500 ns before the probe pulse, a stronger "bleach" pulse interacts with the sample. When the bleaching laser is scanned, it will become resonant with other transitions which start from $v'' = 0$. In that case, the population is removed from the vibrationless ground state, registering as a fluorescence dip for the subsequent probe. The fluorescence dip spectrum is shown in the lower part of Figure 12a,b. Several weak lines in the excitation spectrum do not show up in the OODR spectrum; these are assigned to impurities, which could be a complex with water molecules. Some lines in the OODR spectrum have no

TABLE 3: Transitions Observed in a Supersonic Jet: Labels in Figure 11, Shift $\Delta\nu$ from the Electronic Origin at 28 968 cm^{-1}, and Relative LIF Intensity[a]

label	$\Delta\nu$	intensity	dip	assignment	dip absorbance	dimensionless shift *d*
1	−15.3	0.04	−	−		
2	**0**	**2.28**	+	**origin**	**0.74**[b]	
3	68.5	0.07	−	−		
4	103.2	0.04	−	−		
5	122.7	0.05	−	−		
6	132.2	0.04	−	−		
7	**186.6**	**0.16**	+	**a**	**0.13**	**0.60**
8	**206.8**	**1.25**	+	**b**	**0.41**	**1.05**
9	**228.2**	**0.08**	+	**c**	**0.10**	**0.52**
10	243.4	0.04	−	−		
11	**268.9**	**0.07**	+	**d**	**0.10**	**0.51**
12	295.9	0.05	−	−		
13	**312.6**	**0.13**	+	**e**	**0.23**	**0.79**
14	**350.9**	**0.07**	+	**f**	**0.07**	**0.45**
15	**390.1**	**0.1**	+	**g**	**0.12**	**0.56**
16	412.9	0.24	+	2b		
17	434.2	0.07	+	b + c		
18	**469.5**	**0.2**	+	**h**	**0.27**	**0.85**
19	474.7	0.1	+	b + d		
20	477.7	0.04	+	−		
21	498.0	0.03	+	a + e		
22	516.8	0.06	+	b + e		
23	539.3	0	+	c + e		
24	557.2	0.04	+	b + f		
25	**561.7**	**0.05**	+	**i**	**0.11**	**0.55**
26	**571.1**	**0.02**	+	**j**	**0.05**	**0.35**
27	**578.3**	**0.22**	+	**k**	**0.31**	**0.92**
28	**586.3**	**0.03**	+	**l**	**0.04**	**0.33**
29	595.0	0.12	+	b + g		
30	602.9	0.12	+	2b + a		
31	**607.1**	**0.2**	+	**m**	**0.22**	**0.76**
32	618.9	0.06	+	3b		
33	**633.4**	**0.11**	+	**n**	**0.23**	**0.79**
34	641.0	0.03	+	2b + c		
35	651.3	0.03	−	−		
36	661.9	0.03	−	−		
37	674.5	0.12	+	b + h		
38	680.5	0.04	+	2b + d		
39	684.5	0	+	2a + e		
40	693.5	0.02	+	c + h		
41	**715.6**	**0.01**	+	**o**	**0.09**	**0.48**
42	724.5	0	+	a + 2d, 2a + f, a + c + e		
43	737.0	0.04	+	d + h		
44	741.6	0.06	+	a + b + f, d + h, g + f		
45	752.7	0.01	+	a + i		
46	758.2	0	+	a + j		
47	766.6	0.02	+	3a + b, b + i, 2b + f		
48	784.1	0.06	+	b + k, 2g		
49	792.4	0.02	+	b + l, a + m		
50	799.8	0.03	+	b + g		
51	805.1	0.03	+	3b + a, c + k		
52	812.5	0.05	+	b + m		
53	840.3	0	+	a + d + g, d + j, a + h		
54	847.2	0	+	a + e + f, c + d + f, 2c + g, 2d + e		
55	857.9	0.03	−	−		
56	880.2	0.03	+	2b + h		
57	887.6	0.02	+	3b + d, e + k		
58	940.3	0.02	+	d + h, 2h, e + n		
59	945.6	0.03	+	e + n, b + d + h		
60	973.8	0.01	+	2b + i, 3b + f, a + b + k		
61	988.0	0.06	+	2b + k, b + e + h		
62	1000.4	0	+	a + b + e, a + c + l		
63	1017.3	0.02	+	2b + m, g + n, b + c + k		
64	1044.4	0.03	+	2b + n, h + k, b + c + m		
65	1083.9	0.02	+	b + d + m, 3b + h		
66	1101.7	0.02	+	h + n, b + e + k		
67	1111.5	0.03	+	b + d + n, a + e + m		
68	1120.5	0.03	+	b + e + m, 2h + a		
69	1151.9	0.03	+	2k, 2 h + b		
70	1175.5	0.03	+	b + g + k, 4b + f, 3b + i		
71	1187.3	0.03	+	k + m, 3b + j		
72	1193.6	0.04	+	3b + k, k + m		
73	1208.6	0.03	+	2m, k + n		
74	1316.3	0.03	?	b + h + n, d + h + k		
75	**1331.8**	**0.05**	**?**	**p**	−	**-**
76	1364.8	0.03	?	2k + b		

[a] "Dip" marks whether the line also appears in the OODR spectrum (+) or not (−). All lines with $\Delta\nu \leq 1365$ cm^{-1} are assigned to 16 fundamental frequencies (denoted a, b, c,...) and their combinations. Fundamental transitions are marked in boldface. The absorbance value for the dip signal (relative to an estimate for the 00 transition) is used to estimate the dimensionless shift of the mode, i.e., the displacement of the potential energy minima between S_0 and S_1 relative to the oscillation amplitude of the vibrationless state.[32] [b] Inferred from the value for mode b by using the ratio of LIF intensities.

counterpart in the excitation spectrum, for example those labeled 23 and 53. These lines most likely lead to vibronic states that show fast internal conversion and hence do not result in significant fluorescence.

Table 3 lists the wavenumbers and relative intensities. Lines which appear in the OODR spectra are marked as (+) in the column "dip"; these can be assigned unequivocally to the vibrationless ground state of 4AP. Up to 1400 cm^{-1} above the origin, 16 fundamental frequencies are found which (by themselves and in combination) describe all of the observed "cold" lines.

The origin line is strongest in the spectrum. At low pump intensities the fluorescence excitation spectrum consists essentially of a progression in mode b (206.8 cm^{-1}) and of the fundamentals for modes h (469.5 cm^{-1}) and k (578.3 cm^{-1}). Note that the amplitudes of LIF lines are deceptive because internal conversion becomes significant at excess vibrational energy in S_1. The true amplitudes should be larger, as can be inferred from the OODR spectrum. Here lines no. 8 and 27, for example, have similar strength, whereas by LIF at low pump power their amplitude ratio is 6:1. The OODR dip signal is characterized by an absorbance value in Table 3.

4. Discussion

Dynamic Stokes Shift. The extent of the 4AP Stokes shift is strongly affected by H-bonding.[3,7] For example, methanol and acetonitrile have almost the same solvent polarity, but the dynamic shifts amount to 4300 and 2160 cm^{-1}, respectively (Figure 3). Half of the range in methanol may therefore be attributed to microscopic changes involving the carboxy, amino, and imide groups of 4AP. The question arises whether these changes can be recognized in the time behavior which was shown in Figure 6.

Simple continuum theory ignores the shape of the chromophore, charge distribution, and specific solvent−solute interactions. The chromophore is treated as a point dipole at the center of a spherical cavity (radius r), and the surrounding solvent is replaced by a continuum with dielectric dispersion $\varepsilon(\tilde{\nu})$. One needs the dispersion including all fundamental modes; for liquid methanol this is provided in a convenient form in the Supporting Information. Optical excitation at $t = 0$ increases the dipole moment of the solute instantly, causing the reaction field to change and follow in time.

The relevant calculations were outlined in refs 48 and 49. They result in a normalized relaxation function $C(t)$ and thereby describe the instantaneous emission frequency $\tilde{\nu}(t)$ (approximated by the peak frequency $\tilde{\nu}_p(t)$ of the fluorescence band)

$$\tilde{\nu}(t) = \Delta\tilde{\nu} \cdot C(t) + \tilde{\nu}(\infty) \tag{1}$$

Here $\Delta\tilde{\nu} = 2\tilde{\lambda}_{solv} > 0$ is the spectral range over which the nuclear solvent reorganization is reported and $\tilde{\lambda}_{solv}$ the corresponding reorganization frequency. $\Delta\tilde{\nu}$ must be extracted from experimental results such as in Figure 6, but it may also be calculated if only nonspecific solvation is present. The instantaneous emission frequency is governed by[50]

$$hc\tilde{\nu}(t) = hc\tilde{\nu}^{(np)} - \Delta\tilde{\mathbf{m}} \cdot \mathbf{R}(t) - \frac{1}{2}\Delta\tilde{\alpha} \cdot \mathbf{R}(t)^2 \tag{2}$$

where h is Planck's constant, c the velocity of light, and $\tilde{\nu}^{(np)}$ the emission frequency when only dispersion and induction forces are present. The second term on the rhs is due to dipole/dipole interactions between solute and solvent.[50] In the present treatment the polarizability of 4AP in its ground and excited electronic states is also included; correspondingly, the third term in eq 2 is due to interaction of the induced solute dipole with solvent dipoles. $\Delta\tilde{\mathbf{m}} = f_1^{(el)}\mathbf{m}_1 - f_0^{(el)}\mathbf{m}_0$ is the difference of effective dipole moments in the S_1 and S_0 states of the solute, and similarly $\Delta\tilde{\alpha} = f_1^{(el)}\alpha_1 - f_0^{(el)}\alpha_0$ is the difference of effective isotropic polarizabilities (note that $\mathbf{m}_i$ and α_i refer to the dipole moments and polarizabilities of the isolated solute in the gas phase). Self-consistency of the reaction field, to which the electronic (el) solvent polarization contributes, is achieved by the renormalization factors

$$f_i^{(el)} = \left[1 - 2\frac{n^2 - 1}{2n^2 + 1}\alpha_i\right]^{-1} \tag{3}$$

with solvent refractive index n. Following optical excitation, the instantaneous reaction field $\mathbf{R}(t)$ slides from $\mathbf{R}_0$ to $\mathbf{R}_1$[48] which correspond to the equilibrium with the ground and excited state, respectively. Thus, the spectral range is given by

$$hc\Delta\tilde{\nu} = \Delta\tilde{\mathbf{m}} \cdot (\mathbf{R}_1 - \mathbf{R}_0) + \frac{1}{2}\Delta\tilde{\alpha} \cdot (\mathbf{R}_1^2 - \mathbf{R}_0^2) \tag{4}$$

The stationary reaction field is caused by the molecular dipole

$$\mathbf{R}_i = 2\frac{1}{r^3}\left(\frac{\varepsilon - 1}{2\varepsilon + 1} - \frac{n^2 - 1}{2n^2 + 1}\right)\mathbf{m}_i \tag{5}$$

with static dielectric constant ε of the solvent. For a test let us calculate the spectral range $\Delta\tilde{\nu}$ for solvation of 4AP in acetonitrile. Using the parameters $m_0 = 4.5$ D, $m_1 = 7.1$ D, $\alpha_0 = 16$ Å^3, $\alpha_1 = 18.4$ Å^3, $r = 3.3$ Å,[7,51] we obtain 1730 + 334 cm^{-1} for the dipole/dipole and induced-dipole/dipole terms of eq 4, in agreement with experiment (2160 cm^{-1}). Acetonitrile serves as non-hydroxylic reference solvent to methanol because their polarities are similar (Figure 1).

The spectral dynamics $C(t)$ can be calculated from the autocorrelation function of the fluctuating reaction field $\mathbf{R}(t)$, denoted $\chi(t)$. First, it is useful to consider the difference of the equilibrium reaction fields

$$\mathbf{R}_1 - \mathbf{R}_0 = \frac{2}{r^3}\frac{\varepsilon - n^2}{2n^2 + 1}\left(\frac{n_1^2 + 2}{2\varepsilon + n_1^2}m_1 - \frac{n_0^2 + 2}{2\varepsilon + n_0^2}m_0\right)\mathbf{e} \tag{6}$$

Here the dipole vectors $\mathbf{m}_i = m_i\mathbf{e}$ are taken to be parallel to a unit vector $\mathbf{e}$. The polarizabilities α_0 and α_1 of the solute have been expressed through the Clausius−Mossotti relation

$$\frac{\alpha_i}{r^3} = \frac{n_i^2 - 1}{n_i^2 + 2} \tag{7}$$

In effect, the cavity is considered homogeneously filled with a medium of refractive index n_i. Then, eq 6 is extended into the frequency domain by $\varepsilon \rightarrow \varepsilon(\tilde{\nu})$. In this way a frequency-dependent susceptibility is obtained, and $\chi(t)$ can be reached. Thus, the dynamics of the dipole/dipole contribution (second term in eq 2) is described.[52] Finally, from $\chi(t)$ the desired $C(t)$ is calculated.[48] The induced-dipole/dipole contribution (third term) slows down the initial part of the shift, but this effect is relatively small with 4AP.

Simulations should help establish the dielectric point of view. Specifically, we intend to show that the relaxation curve (Figure 6) can be described completely with the set of parameters which reflects the current state of 4AP research.[7,51] Figure 13 shows the spectral density of dipolar solvation by methanol, extending to the Stokes ($\tilde{\nu} > 0$) and anti-Stokes sides (black line). Cosine Fourier transformation followed by normalization gives $C(t)$. In this context, it is important to treat the limited time resolution correctly. The temporal apparatus function is represented in the

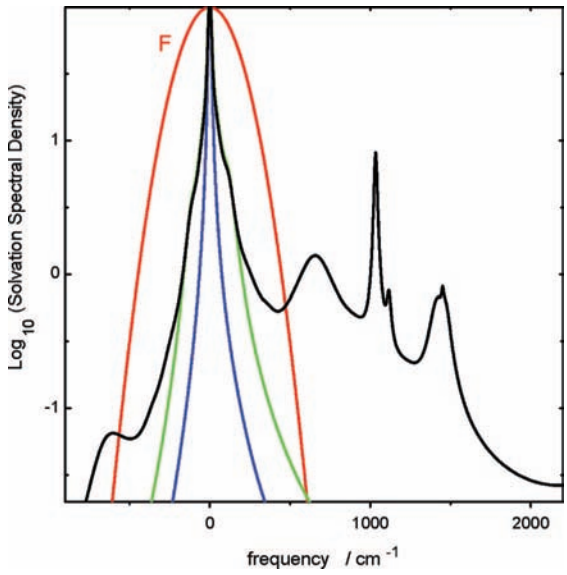

Figure 13. Spectral density for dipole/dipole solvation, calculated by simple continuum theory (eq 6) from the dielectric dispersion $\varepsilon(\tilde{\nu})$ of liquid methanol at 25 °C (black line). Only the lower half of the needed frequency range is shown. The polarizability of 4AP in the excited state is $\alpha_1 = 18.2$ Å^3. The experimental time resolution (85 fs fwhm) leads to the Gaussian filter F (red). The spectral densities due to the "dielectric" modes and to the additional FIR modes up to 120 cm^{-1} are represented by the blue and green lines, respectively.

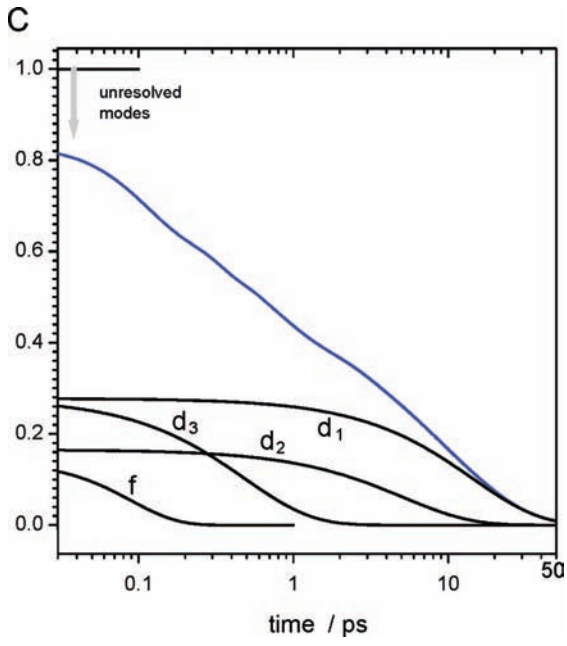

Figure 14. Solvation relaxation function $C(t)$ for 4AP, calculated from the dielectric disperion of methanol with $\alpha_1 = 18.2$ Å^3. An initial drop is due to modes which cannot be resolved at the given experimental resolution. On the logarithmic time scale, dielectric modes d_1 and d_2 known from microwave spectroscopy of the liquid can be distinguished from a fast dielectric mode d_3 and a FIR mode f at 116 cm^{-1} (black lines, see Supporting Information).

frequency domain by a Gaussian filter which drops to 50% at 173 cm^{-1} (red line). An intermolecular mode of methanol, which in the FIR spectrum of the liquid[53] has a broadband at 116 cm^{-1}, is seen as a shoulder in the spectral density, and it is expected to be time resolved by our fluorescence upconversion measurement. Modes outside of the filter window, for example the sharp C−O or broad O−H stretching bands, cannot be resolved. Instead, they appear as an instantaneous drop from $C(0) = 1$ to an initial measurable value $C(0^+)$.[54] The latter is obtained as the integral over the filter-weighted spectral density, relative to the integral over the spectral density itself.

The measurement points $\tilde{\nu}(t)$ are now compared to the simulations by fitting them with eq 1. The parameters α_1 and $\Delta\tilde{\nu}$ are both allowed to adjust freely (the other parameter values above are kept), resulting in $\alpha_1 = 18.2 \pm 1.0$ Å^3 with correlated $\Delta\tilde{\nu} = 4410 \mp 290$ cm^{-1}. Thus, a value for α_1 is returned which is close to the previous estimate.[51] The optimal description is shown as blue lines in Figure 6. The deviation of the measured points (49 cm^{-1} rms) is only marginally larger compared to the triexponential fit (green lines) which was mentioned in the Results section. The match by continuum theory extends over the entire time range 0.10−40 ps, and especially the exponential regime change around 1.3 ps is clearly expressed. Figure 14 provides a decomposition of $C(t)$ into four Brownian oscillator modes, which may be associated (see Supporting Information) with three modes observed for dielectric relaxation[55] and the far-infrared band[53] at 116 cm^{-1} of pure methanol. These findings suggest that nonspecific polar solvation is being observed here. Not only the shape of the measured $\tilde{\nu}(t)$ data set agrees well with continuum theory but also the extrapolation $t \rightarrow 0$ matches with the observations. It implies that polar solvation sets in an $\Delta\tilde{\nu} + \tilde{\nu}(\infty) = 22\,960$ cm^{-1}, in agreement with the value $\tilde{\nu}(0) = 22\,850$ cm^{-1} from the "spectroscopic time-zero analysis. There is no need to attribute part of the reorganization energy to H-bonding with specific dynamics, distinct from polar dynamics. (Contrast this with the multiexponential description of $\tilde{\nu}(t)$, Table 2, which upon extrapolation $t \rightarrow 0$ misses 1120 cm^{-1} of the dynamic Stokes shift;[13] Figure 6.) It follows that fluorescing 4-aminophthalimide reports polar solvation faithfully, at least in methanol, despite H-bonding.

Spectral broadening upon going from 2-methylbutane to methanol solution can also be explained by polar solvation. On one hand, it is characterized through stationary spectroscopy, as convolution of the $S_1 \leftarrow S_0$ absorption line shape in 2-methylbutane by a Gaussian $\sim\exp(-\tilde{\nu}^2/2\tilde{\delta}^2)$ with $\tilde{\delta}_{abs} = 1010$ cm^{-1} On the other hand, it may be estimated from the dynamic reorganization frequency $\Delta\tilde{\nu}$ as[56]

$$\tilde{\delta}_{shift} = \sqrt{\Delta\tilde{\nu} \cdot k_B T/hc} \qquad (8)$$

Here k_B is Boltzmann's constant and h Planck's constant, and T is the temperature. Using the full dynamic shift $\Delta\tilde{\nu} = 4300$ cm^{-1}, we find $\tilde{\delta}_{shift} = 940$ cm^{-1}, i.e., 70 cm^{-1} below $\tilde{\delta}_{abs}$ at the limit of the confidence interval for time-zero analysis. For an explanation of this discrepancy, let us compare the stationary emission spectra in 2-methylbutane and methanol also. When the emission line shape in 2-methylbutane is properly shifted and then broadened by only $\tilde{\delta}_{fls} = 300$ cm^{-1}, one obtains the simulated fluorescence quantum distribution which is shown as a red line in Figure 3. The broadening diminishes as solvation by methanol proceeds, and this is reflected by the time-dependent width $\Delta(t)$ of the evolving fluorescence band (Figure 7). Evidently, intramolecular modes are coupled to the solvent coordinate, but we can only speculate on the mechanisms: by nonlinear interaction with the reaction field,[57] or indeed specifically through H-bonds.[7] In either case, a systematic difference is implied between $\tilde{\delta}_{abs}$ and $\tilde{\delta}_{shift}$.

Finally, for this part, the intramolecular reorganization energy in 2-methylbutane, $\tilde{\lambda}_{intra} \approx 2025$ cm^{-1}, is discussed. This value can be placed into the context of the jet spectroscopy above. There 16 modes $\tilde{\nu}_j$ (out of 48) were determined, and the dimensionless displacements d_j for 15 modes were estimated from the relative intensities of the OODR lines (Table 3). The

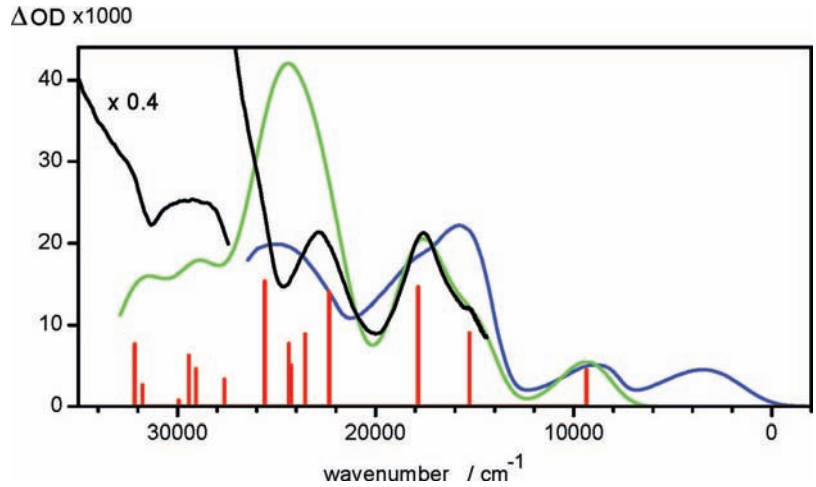

Figure 15. Assignment of the ESA spectrum. Black, measurement at $t = \infty$; blue, shifted ground-state absorption; green, spectrum from broadening the calculated A′ transitions (vertical bars, see text).

classical intramolecular reorganization energy for these modes is $\sum_{j=1}^{15} \tilde{\nu}_j d_j^2/2 = 1440$ cm^{-1}. Assuming that the mode at 1331.8 cm^{-1} is responsible for the remaining contribution $\tilde{\nu}_{16} d_{16}^2/2$ to $\tilde{\lambda}_{\text{intra}}$, we find $d_{16} \approx 0.95$. In addition, we simulated the absorption and emission line shapes in 2-methylbutane with Brownian oscillators.[58,59] A high-frequency intramolecular mode of 1350−1400 cm^{-1} is again required, with dimensionless displacement 1.5−1.7. Single-level fluorescence from 3AP in a supersonic jet showed activity in a mode at 1389 cm^{-1}, ascribed to a C═C stretching vibration, with an estimated displacement ≈1.[32] We conclude that the major part of the intramolecular reorganization can be represented by the modes collected in Table 3. An interesting aspect of the reorganization between the S_0 and S_1 states is a long progression in the fluorescence excitation spectrum with vibrational spacing of 206.8 cm^{-1}, mode b in Table 3. Our quantum-chemical calculations predict a planar S_1 state, whereas the amino group has a pyramidal conformation in the S_0 state (see Supporting Information). Correspondingly, mode b is assigned to out-of-plane motion of the amino group (rather than to in-plane wagging involving the >C═O groups[60]) and the progressional spacing to double quantum transitions.

The excited-state absorption spectrum of 4AP in methanol (Figure 11) was obtained as a side result in section 3.2. A blue-shift of the ESA band at 560 nm reflects a decrease of dipole moment upon excitation $S_n \leftarrow S_1$.[25,26] Since the band is neither sharp nor prominent, however, it cannot be used to measure solvation dynamics as suggested for other probes.[26] It is interesting to discuss the ESA spectrum for other reasons instead.

The location of electronic states can be estimated in conjunction with quantum-chemical calculations. For this purpose the ESA spectrum is plotted on an energy scale in Figure 15 (black lines, referring to $t = \infty$). The ground-state absorption spectrum is shown shifted by −23 550 cm^{-1} (blue line). Before proceeding, remember that the TD-DFT transition energies, as reported here, refer to the isolated molecule constrained to planarity. Disregarding the limitations of the method and of its implementation, the calculations agree with experiments in that $S_2 \equiv A''(1)$ is well separated from $S_1 \equiv A'(1)$; only the latter is expected to be populated by excitation at 403 nm. Transition moments with sizable oscillator strength point essentially in the molecular plane, and this is why the ESA spectrum involves transitions only which can be classified $A'(i) \leftarrow A'(1)$. The higher states $i = 3,4$ are readily identified by comparison with

SCHEME 2: Surrogate Base Pair (R = 2′-Deoxyribose) Suggested for Measuring Dielectric Relaxation around Double-Stranded DNA

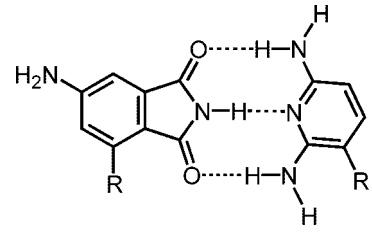

$A'(i) \leftarrow A'(0)$. The calculations predict a ratio of oscillator strengths $f_{40}/f_{30} \approx 0.45$ for ground-state absorption, which is inverted to $f_{41}/f_{31} \approx 1.62$ for excited-state absorption. With this knowledge, the blue line in Figure 15 was adjusted, thus locating the zero point for the free energy axis (1260 cm^{-1} below the electronic origin in methanol). The calculated pattern of $A'(i) \leftarrow A'(1)$ transitions (vertical bars) and an associated absorption envelope are also shown in the figure (green line; log-normals with $\Delta = 1500$ cm^{-1}, $\gamma = 0.16$). The calculated transition frequencies had to be increased by +2900 cm^{-1} for a match with experiment. The characteristic structure of the observed ESA spectrum, especially the minimum around 20 000 cm^{-1}, is well represented by the calculations. We conclude that the states A′(4) and A′(3) are reasonably isolated from their neighbors. The peak of the $A'(4) \leftarrow A'(1)$ transition at 568 nm is convenient for time-resolved resonance Raman spectroscopy in the excited state.[61,62] In that way, one could follow the structural relaxation, including H-bonds, more directly.

5. Concluding Remarks

We presented femtosecond time-resolved emission and transient absorption spectra of the popular solvatochromic probe 4-aminophthalimide (4AP) in methanol solution at room temperature. We also provided stationary spectra in a nonpolar reference solvent, results from supersonic jet spectroscopy, and calculations by density functional theory, CIS, and CASSCF/MC-QDPT2. Together they support the interpretation of the time-resolved data. The main conclusion of this work is that, despite the well-known fact that Stokes shifts of 4AP are nearly 2-fold larger in hydrogen bond donating solvents compared to polar aprotic solvents, the dynamic Stokes shift in methanol is well described solely by nonspecific solvation.

This surprising result should be of interest to many researchers working in the area of solution-phase dynamics. For example, C-nucleosides of 4-aminophthalimide and 2,6-diaminopyridine[63] could be incorporated into double-stranded DNA by conventional synthesis protocols. The surrogate base pair (Scheme 2) may then be used to measure dielectric relaxation. Corresponding work is in progress in several laboratories.

Acknowledgment. We are grateful to A. Neugebauer and Dr. B. Ziemer for the X-ray structure, and to the Fonds der Chemischen Industrie and the Deutsche Forschungsgemeinschaft for support.

Supporting Information Available: Structures of 4AP in S_0 and S_1, parameters for stationary spectra in the condensed phase, dielectric dispersion of methanol in a useful form, description of $C(t)$ by Brownian oscillators. This material is available free of charge via Internet at http://pubs.acs.org

References and Notes

(1) Soujanya, T.; Krishma, T. S. R.; Samanta, A. *J. Phys. Chem.* **1992**, *96*, 8544.
(2) Saroja, G.; Ramachandram, B.; Saha, S.; Samanta, A. *J. Phys. Chem. B* **1999**, *103*, 2906.
(3) Chapman, C. F.; Maroncelli, M. *J. Phys. Chem.* **1991**, *95*, 9095.
(4) Paul, A.; Samanta, A. *J. Phys. Chem. B* **2007**, *111*, 4724.
(5) Barja, B. C.; Chesta, C.; Atvars, T. D. Z.; Aramendia, P. *J. Phys. Chem. B* **2005**, *109*, 16180.
(6) Noukakis, D.; Suppan, P. *J. Lumin.* **1991**, *47*, 285. Spectra were remeasured for the figure, and peak positions of the lineshapes were corrected for dispersion shifts (reference solvent = 2-methylbutane). Regression lines were obtained from data points for nonprotic solvents except cyclohexane and dioxane. Slopes are −1936 cm^{-1} for absorption and −3200 cm^{-1} for fluorescence.
(7) Dobek, K. *Photochem. Photobiol. Sci.* **2008**, *7*, 361.
(8) Fee, R. S.; Maroncelli, M. *Chem. Phys.* **1994**, *183*, 235.
(9) Krystkowiak, E.; Dobek, K.; Maciejewski, A. *J. Photochem. Photobiol. A—Chem.* **2006**, *184*, 250.
(10) Harju, T.; Huizer, A. H.; Varma, C. A. G. O. *Chem. Phys.* **1995**, *200*, 215.
(11) Das, S.; Datta, A.; Bhattacharyya, K. *J. Phys. Chem. A* **1997**, *101*, 3.
(12) Bhattacharya, B.; Samanta, A. *Chem. Phys. Lett.* **2007**, *442*, 316.
(13) Chapman, C. F.; Fee, R. S.; Maroncelli, M. *J. Phys. Chem.* **1995**, *99*, 4811.
(14) Laitinen, E.; Salonen, K.; Harju, T. *J. Chem. Phys.* **1996**, *104*, 6138.
(15) Laitinen, E.; Salonen, K.; Harju, T. *J. Chem. Phys.* **1996**, *105*, 9771.
(16) Datta, A.; Mandal, D.; Pal, S. K.; Das, S.; Bhattacharyya, K. *J. Mol. Liq.* **1998**, *77*, 121.
(17) Mandal, D.; Datta, A.; Pal, S. K.; Bhattacharyya, K. *J. Phys. Chem. B* **1998**, *102*, 9070.
(18) Mondal, S. K.; Roy, D.; Sahu, K.; Sen, P.; Karmakar, R.; Bhattacharyya, K. *J. Photochem. Photobiol. A—Chem.* **2005**, *173*, 334.
(19) Haacke, S.; Taylor, R. A.; Bar-Joseph, I.; Brasil, M. J. S. P.; Hartig, M.; Deveaud, B. *J. Opt. Soc. Am. B* **1998**, *15*, 1410.
(20) Schanz, R.; Kovalenko, S. A.; Kharnalov, V.; Ernsting, N. P. *Appl. Phys. Lett.* **2001**, *79*, 566.
(21) Kovalenko, S. A.; Schanz, R.; Senyushkina, T. A.; Ernsting, N. P. *Phys. Chem. Chem. Phys.* **2002**, *4*, 703.
(22) Zhao, L.; Lustres, L. P.; Farztdinov, V.; Ernsting, N. P. *Phys. Chem. Chem. Phys.* **2005**, *7*, 1716.
(23) Gustavsson, T.; Cassara, L.; Gulbinas, V.; Gurzadyan, G.; Mialocq, J. C.; Pommeret, S.; Sorgius, M.; van der Meulen, P. *J. Phys. Chem. A* **1998**, *102*, 4229.
(24) Horng, M. L.; Gardecki, J. A.; Papazyan, A.; Maroncelli, M. *J. Phys. Chem.* **1995**, *99*, 17311.
(25) Kovalenko, S. A.; Ruthmann, J.; Ernsting, N. P. *Chem. Phys. Lett.* **1997**, *271*, 40.
(26) Karunakaran, V.; Pfaffe, M.; Ioffe, I.; Senyushkina, T.; Kovalenko, S. A.; Mahrwald, R.; Farztdinov, V.; Sklenar, H.; Ernsting, N. P. *J. Phys. Chem.* **2008**, *112*, 4294.
(27) Andreatta, D.; Sen, S.; Lustres, J. L. P.; Kovalenko, S. A.; Ernsting, N. P.; Murphy, C. J.; Coleman, R. S.; Berg, M. A. *J. Am. Chem. Soc.* **2006**, *128*, 6885.
(28) Andreatta, D.; Lustres, J. L. P.; Kovalenko, S. A.; Ernsting, N. P.; Murphy, C. J.; Coleman, R. S.; Berg, M. A. *J. Am. Chem. Soc.* **2005**, *127*, 7270.
(29) Pryor, B. A.; Palmer, P. M.; Chen, Yu.; Topp, M. R. *Chem. Phys. Lett.* **1999**, *299*, 536.
(30) Mühlpfordt, A.; Schanz, R.; Ernsing, N. P.; Fartzdinov, V.; Grimme, S. *Phys. Chem. Chem. Phys.* **1999**, *1*, 3209.
(31) Asimov, M.; Ernsting, N. P. *J. Lumin.* **1983**, *28*, 119.
(32) Gulis, I. M.; Komyak, A. I.; Saechnikov, K. A.; Tsvirko, V. A. *Zh.Prikl. Spektrosk.* **1989**, *50*, 385.
(33) Dobryakov, A. D.; Ernsting, N. P. In *Analysis and Control of Ultrafast Photoinduced Reactions*; Kühn, O., Wöste, L., Eds.; Springer Series in Chemical Physics, Vol. *87*; Springer: Heidelberg, Germany, 2007; p 689.
(34) Kovalenko, S. A.; Dobryakov, A. L.; Ruthmann, J.; Ernsting, N. P. *Phys. Rev. A* **1999**, *59*, 2369.
(35) Kessler, A.; Slenczka, A.; Seiler, R.; Dick, B. *Phys. Chem. Chem. Phys.* **2001**, *3*, 2819.
(36) Seiler, R.; Kensy, U.; Dick, B. *Phys. Chem. Chem. Phys.* **2001**, *3*, 5373.
(37) Schmidt, M. W.; Baldridge, K. K.; Boatz, J. A.; Elbert, S. T.; Gordon, M. S.; Jensen, J. H.; Koseki, S.; Matsunaga, N.; Nguyen, K. A.; Su, S. J.; Windus, T. L.; Dupuis, M.; Montgomery, J. A. *J. Comput. Chem.* **1993**, *14*, 1347. GordonM. S.; SchmidtM. W. In *Theory and Applications of Computational Chemistry, the first forty years*; Dykstra, C. E., Frenking, G., Kim, K. S., Scuseria, G. E., Eds.; Elsevier: Amsterdam, 2005.
(38) Granovsky, A. A.,PC GAMESS version 7.0, http://classic.chem.msu.su/gran/gamess/index.html. Nemukhin, A. V.; Grigorenko, B. L.; Granovsky, A. A. *Moscow Univ. Chem. Bull.* **2004**, *45* (No. 2), 75.
(39) Nakano, H. *J. Chem. Phys.* **1993**, *99*, 7983. Nakano, H. *Chem.Phys.Lett.* **1993**, *207*, 372.
(40) Hirayama, S.; Phillips, D. *J. Photochem.* **1980**, *12*, 139.
(41) Siano, D. B.; Metzler, D. E. *J. Chem. Phys.* **1969**, *51*, 1856.
(42) Since the excitation pulse is short, eq 3 of ref 8 must be integrated over $\tilde{\nu}_{exc}$ also.
(43) Marcus, Y.; Kamlet, M. J.; Taft, R. W. *J. Phys. Chem.* **1988**, *92*, 3613.
(44) Regarding the spectral position of the pump pulse on the red edge of the absorption band, excitation of 4AP in acetonitrile centered at 388 nm is equivalent to excitation in methanol centered at 403 nm. The former leads to a time-zero fqd which peaks at 23 550 cm^{-1}. The peak of the stationary fqd in acetonitrile is observed at 21 390 cm^{-1}.
(45) Angle by which the H_2N plane deviates from the plane of non-hydrogen atoms.
(46) Dreuw, A.; Head-Gordon, M. *Chem. Rev.* **2005**, *105*, 4009.
(47) Since nonexponentiality is expected at early time, the triexponential fit should properly be restricted to $t > 1$ ps. The same rmsd of 40 cm^{-1} is found for the restricted time interval.
(48) Lustres, J. L. P.; Kovalenko, S. A.; Mosquera, M.; Senyushkina, T.; Flasche, W.; Ernsting, N. P. *Angew. Chem. Int. Ed.* **2005**, *44*, 5635.
(49) Ruthmann, J.; Kovalenko, S. A.; Ernsting, N. P. *J. Chem. Phys.* **1998**, *109*, 5466.
(50) Matyushov, D. *V.; J. Chem. Phys.* **2001**, *115*, 8933.
(51) Bakshiev, N. G. *Opt. Spektrosk.* **2001**, *91*, 721.
(52) Previously we used the susceptibility $\propto(\varepsilon(\tilde{\nu})-1)/(2\varepsilon(\tilde{\nu})+n_{cav}^2)$ with an effective refractive index n_{cav} for the cavity,[48] which is obtained when $m_0 = 0$, for example.
(53) Bertie, J. E.; Zhang, S. L.; Eysel, H. H.; Baluja, S.; Ahmed, M. K. *Appl. Spectrosc.* **1993**, *47*, 1100.
(54) At the given time resolution, the emission frequency $\tilde{\nu}(0^+) = \Delta\tilde{\nu}\, C(0^+) + \tilde{\nu}(\infty)$ would be measured at delay time $t = 0$ if solvent Raman signal were absent. In practice, only at $t = 100$ fs did the solvent Raman signal become small enough so that the the peak frequency can be determined reliably.
(55) Barthel, J.; Bachhuber, K.; Buchner, R.; Hetzenauer, H. *Chem. Phys. Lett.* **1990**, *165*, 369.
(56) Marcus., R. A. *J. Chem. Phys.* **1965**, *43*, 1261.
(57) Matyushov, D. V.; Newton, M. D. *J. Phys. Chem. A* **2001**, *105*, 8516.
(58) Nibbering, E. T. J.; Wiersma, D. A.; Dubben, K. *Chem. Phys.* **1994**, *183*, 167.
(59) Mukamel, S. *Principles of Nonlinear optical Spectroscopy*; Oxford University: New York, 1995.
(60) Chen, Y.; Topp, M. R. *Chem. Phys. Lett.* **2002**, *355*, 270.
(61) Yoshizawa, M.; Kurosawa, M. *Phys. Rev. A* **1999**, *61*, 013808.
(62) Kukura, P.; Yoon, S.; Mathies, R. A. *Anal. Chem.* **2006**, *78*, 5952.
(63) Sun, Z.; Ahmed, S.; McLaughlin, L. W. *J. Org. Chem.* **2006**, *71*, 2922.

JP807605B